Anisotropic Growth of a Nickel Trimer Formed on a Highly-Stepped TiO_2(110) Surface

Hiromitsu Uehara,[a] Muhammad Haneef bin Hanaffi,[a] Yuichiro Koike,[a] Keisuke Fujikawa,[a] Shushi Suzuki,[b] Hiroko Ariga,[a] Satoru Takakusagi,[a] Wang-Jae Chun, [c] Yasuhiro Iwasawa,[d] and Kiyotaka Asakura[*,a]

[a] Catalysis Research Center, Hokkaido University, Kita 21 Nishi 10, Kita Sapporo 001-0021, Japan

[b] Departments of Engineering Science and Crystalline Materials Science, Graduate School of Engineering, Nagoya University, Nagoya 464-8603, Japan

[c] Graduate School of Arts and Sciences, International Christian University, Mitaka, Tokyo 181-8585, Japan

[d] Innovation Research Center for Fuel Cells, Department of Engineering Science, Graduate School of Information Engineering Science, The University of Electro-Communications, 1-5-1 Chofugaoka, Chofu, Tokyo182-8585, Japan

*Corresponding author

Phone and Fax: 81-11-706-9113

E-mail address: *askr@cat.hokudai.ac.jp*

Abstract

The structures of Ni clusters formed on a highly-stepped TiO_2(110) surface were studied by polarization-dependent total reflection fluorescence X-ray absorption fine structure analysis. When 0.8 monolayers of Ni were deposited, three-dimensional Ni clusters with 1–2 nm diameters and heights less than 1 nm were formed. Conversely, when 0.07 monolayers of Ni were deposited, an anisotropic Ni trimer with a Ni–Ni distance of 0.260 nm was created at the [001] step. We revealed that the surface modification to enhance the metal-anion interaction can control the deposited metal structure.

1. Introduction

Small transition metal clusters are used in many applications such as catalysts, sensors, fuel cells, magnetic devices, and optical devices, as well as in medicine [1-6]. The properties of the clusters largely depend on their size and shape. It is becoming possible to control these parameters precisely on an atomic scale using ligands, protecting polymers, structure directing agents and oxide

surfaces [6-10]. Coordinately unsaturated metastable clusters are stabilized by metal oxide surfaces and are used as supported metal catalysts [11]. Attachment of organometallic complexes provides well-defined and unsaturated metal monomers, dimers, trimers, and clusters [12, 13]. Although the structures of such small transition metal clusters have been characterized by many spectroscopic techniques, their three-dimensional molecular structures are not easily determined because the oxide supports are usually in powder form. In this respect, studies using the metal species on single crystal oxides or single crystal oxide films are necessary [14-20].

When the polarization-dependent total reflection fluorescence X-ray absorption fine structure (PTRF-XAFS) technique is applied to a single crystal oxide, three-dimensional structural information can be obtained using the polarization dependence of the XAFS amplitude [21, 22]. For example, Mo species were deposited on the TiO_2(110) surface, which has an anisotropic structure [23], under various conditions and studied using PTRF-XAFS [22, 24-27]. Mo monomers, dimers, and chains were produced on this surface through the interaction with surface oxygen atoms. Late transition metals, on the other hand, experience weaker interaction with the supports. We have applied the PTRF-XAFS technique to Ni and Cu species deposited on oxide single crystals such as Al_2O_3(0001) and TiO_2(110) [28-33]. Accordingly, we showed for Ni that, depending on the deposition amount, either monoatomically dispersed Ni species attached to the steps at 0.02 ML or two-dimensional, well-defined Ni clusters were formed on the terrace of the TiO_2(110) with Ni fcc(110) parallel to the surface at 0.2 ML. We concluded that the Ni–O bonding was important to obtain metal monomers and two-dimensional metal clusters [28-32]. However, Zhou et al. observed three-dimensional metal nanoparticle growth on the step edge [33]. In our previous paper, we assumed that the different growth mode might be due to the different step density [32]. Surface defects such as steps and oxygen vacancies on oxide surface may play an important role in determining the structure of surface metal species [34-44].

In the present work, PTRF-XAFS was performed to ascertain the structure of Ni species on a highly-stepped TiO_2(110) surface, which had a higher step density than that of our previous study [32], to identify the effect of step size on the structure of Ni. We discuss the metal–support interaction as well as the way to control the metal structures on the oxide surface.

2. Experimental

2.1. Materials and Sample Preparation

An optically polished rutile TiO_2(110) single crystal (20 mm × 20 mm × 1 mm; Earth Jewelry Co., Kobe, Japan) was heated at 1273 K for 1 h in air to remove carbon contaminates. The sample was further treated using several cycles of Ar^+ sputtering (2 kV, 2.8 μA) and annealing at 900 K for 10 min in a ultrahigh vacuum (UHV) system (base pressure was 1×10^{-8} Pa) [21]. Consequently, we obtained a clean and well-ordered TiO_2(110) surface. The sample was subsequently sputtered again

with Ar^+ (2 kV, 2.8 μA) for 10 min and the surface was then annealed at 873 K. This procedure resulted in a diffuse (1 × 1) LEED pattern (Figure S1 in the supplementary material) and highly stepped surface (Figure S2). No C1s was detected in the XPS as shown in Figure S3. As shown in Figure 2, a shoulder structure was found in the Ti $2p_{3/2}$ peak at 456.5 eV indicating the presence of Ti^{3+} and oxygen defects [23]. Ni was then evaporated by resistive heating from a tungsten filament wrapped with a Ni wire. The amount of Ni deposited on the highly-stepped TiO_2(110) surface was also estimated from the XPS spectra of Ni $2p_{3/2}$. Here, 1 monolayer (ML) was defined as 5.2×10^{14} atoms·cm^{-2} corresponding to the TiO_2(110)-(1 × 1) unit cell. Two different samples with different Ni coverage, 4.2×10^{14} atoms·cm^{-2} (0.8 ML) and 3.6×10^{13} atoms·cm^{-2} (0.07 ML) were separately prepared. The thus-prepared sample was then transferred using a transfer chamber to the XAFS measurement chamber under UHV conditions[27].

2.2. PTRF-XAFS Measurements

The PTRF-XAFS measurements were carried out at BL9A of Photon Factory in the Institute of Material Structure Science (KEK-IMMS-PF, Tsukuba, Japan), under operating conditions of 2.5 GeV and 400 mA. The X-rays were monochromatized using a Si(111) double-crystal monochromator. Because glancing incidence angle was used, the beam size of the X-ray on the sample was regulated using a 0.4-mm pinhole before the I_0 ionization chamber to reduce undesirable irradiation of areas other than the sample surface. The fluorescence X-rays were detected with a 19-element, pure Ge solid-state detector (GL0110S; Canberra, Meriden, Connecticut, USA). The measurement chamber was equipped with a six-axis goniometer to adjust the total reflection conditions and sample orientation against the electric vector of the incident X-ray. PTRF-XAFS measurements were carried out in three different orientations against the electric vector of the incident X-rays, i.e., two parallel orientations to the surface, *E*//[001] and *E*//[$1\bar{1}0$], and one perpendicular orientation to the surface *E*//[110] [45].

2.3. Extended x-ray absorption fine structure(EXAFS) Analysis

The EXAFS analyses were carried out using a REX 2000 software. Preliminary analysis was carried out by the curve fitting method using the following equation:

$$k^{n}\chi_{obs}(k) = k^{n-1}\sum_{j} N_{eff,j}\frac{SF_j(k)e^{-2\sigma_j^2 k^2}}{r_j^2}\sin(2kr_j + \phi_j(k)) \quad , \tag{1}$$

where k, $\chi_{obs}(k)$, $N_{eff,j}$, S, r_j, σ_j, $F_j(k)$, and $\phi_j(k)$ are the wavenumber, observed XAFS oscillation, effective coordination number of j-th shell, reduction factor, bond distance, Debye–Waller factor,

backscattering amplitude functions, and phase shift of the *j*-th shell, respectively. Note that $N_{\mathrm{eff},j}$ has a polarization dependence that is expressed as

$$N_{\mathrm{eff},j} = \sum_{ij} 3\cos^2\theta_{ij} \quad , \tag{2}$$

where θ_{ij} is an angle between the polarization direction of the electric vector and the bond direction of the *i*-th bond in the *j*-th shell.

The extracted EXAFS oscillations were simulated based on a real space structural model using the FEFF (v8.40) software package [46]. Multiple scattering was included up to triple one. The goodness of the fit was evaluated using the following equation:

$$R = \sqrt{\frac{1}{\mathrm{N_{data}}} \sum_{k} \frac{(\chi_{\mathrm{obs}}(k) - \chi_{\mathrm{cal}}(k))^2}{\varepsilon(k)^2}} \quad , \tag{3}$$

where $\mathrm{N_{data}}$ is the number of data points, $\chi_{\mathrm{cal}}(k)$ is the calculated EXAFS oscillation, and $\varepsilon(k)$ is the error. We used the standard deviation of each measurement point as the error. If the *R* value of a model structure was less than 1, the EXAFS oscillation could be reproduced by the structure in real space within the experimental error range.

3. Results and Discussion

3.1. X-ray Absorption Near Edge Structure (XANES) Spectra of Ni Species on the highly-stepped TiO_2(110) Surfaces

Figure 3 shows the XANES spectra of Ni species on the highly-stepped TiO_2(110) surface. The edge positions of the XANES spectra for the 0.8 ML sample were the same as those of Ni foil, as shown in Figure 3b–d. However, the spectral features above the edge were less clear, indicating that the metallic cluster was formed but the size of cluster was small [47]. The polarization dependence was not as large as that found for the flatter TiO_2(110) surface, indicating the presence of the more isotropic Ni metallic species. On the contrary, the 0.07 ML Ni species showed different features. Although the edge positions of the 0.07 ML samples were almost the same as those of the Ni foil and 0.8 ML samples, the Ni first edge peaks appearing at 8348 eV were stronger and sharper than those of the 0.8 ML samples, indicating the presence of more oxidized Ni species. In addition, the edge peak height of the 0.07 ML sample was slightly lower in the [001] direction. Recently Domenihini et al. reported the Ni showed the electron transfer to the Ti^{4+} only at low coverage, well corresponding to our observations.[48]

3.2. Structural Analysis of Ni Clusters at a Coverage of 0.8 ML

Figure 4a shows the normalized Ni K edge PTRF-EXAFS oscillations, $\chi(k)$, of the 0.8 ML sample. The main peak positions for all directions correspond well with those of the Ni foil (bottom of Figure 4a), although the oscillations had less defined structures and smaller amplitudes. Thus, this indicates that small Ni clusters were formed on the TiO_2(110) surface. Curve fitting analysis showed that the Ni–Ni distance was 0.246 nm. There was little polarization dependence in the two directions parallel to the TiO_2(110) surface and a slightly smaller amplitude was found in the [110] direction. We have previously reported a similar Ni structure on a clean and well-ordered TiO_2(110) surface with 0.8 MLs, where the Ni clusters had a hemispheroidal shape with dimensions 1.3 nm × 1.7 nm × 0.6 nm [32]. On the present TiO_2(110) surface, a three-dimensional Ni cluster of about 1.0 ± 0.5 nm in lateral size and less than 0.8 ± 0.4 nm in height was stabilized. Therefore, we concluded that the steps on the substrate reduced the anisotropy in the diffusion to provide isotropic Ni cluster compared with a flat surface.

3.3. Structural Analysis of Ni Clusters at a Coverage of 0.07 ML

We decreased the deposited amount of Ni to 0.07 ML. Figure 4b shows the PTRF-XAFS oscillation of the 0.07 ML sample deposited on a highly-stepped TiO_2(110) surface. The EXAFS oscillation shows a clear polarization dependence. The EXAFS oscillations of the E//[$1\bar{1}0$] and E//[110] directions were attenuated to a greater extent with increasing k than that of the E//[001] direction in the high k region. Moreover, the oscillations parallel to the [110] and [$1\bar{1}0$] directions showed quick damping, indicating that the Ni was bonded to a “light-element” in the [110] and [$1\bar{1}0$] directions. Conversely, in the [001] direction, the oscillations had shorter periods in the high k region, indicating the presence of Ni–Ni. A preliminary single shell curve fitting analysis indicated that the main contribution was a Ni–Ni interaction at 0.260 nm with an effective coordination number, N_{eff} of 4 ± 1 in the [001] direction. It should be noted that the effective coordination number is $3\cos^2\theta$ times larger than the real one. We did not observe a Ni–Ni interaction in the other directions, indicating that the Ni–Ni bond was directed to the [001] direction. The real coordination number in the [001] direction was, hence, 1.3 ± 0.3. The presence of one-dimensional Ni clusters located between the bridging oxygen row and above the in-plane oxygen atoms is possible, as suggested by Onishi [49]. Based on the curve fitting analysis, we constructed the model structure of an anisotropic Ni cluster in real space and optimized it based on theoretical XAFS calculations using the FEFF program. A flat terrace site poorly reproduced the XAFS oscillations; the Ni chain in the trough between the bridging oxygen rows should have a Ni–Ti distance of 0.25 nm in the [110] and [$1\bar{1}0$] directions when the Ni–O distance is fixed at less than 0.21 nm [28]. The step edge was the next possible site where Ni–O could be observed both in the [110] and [$1\bar{1}0$] directions [29, 31]. We have demonstrated that Ni monomer species attached onto the step at very low coverage (ca. 0.02 ML)

[31]. It should be mentioned that Chen and Tanner [33, 50, 51] also reported the selective nucleation of Ni and Cu clusters at the step sites of the TiO_2(110).

We were able to reproduce the data shown in Figure 5 by fixing one-dimensional Ni trimers at the [001] steps (Figure 6). The values of goodness for the fit, *R*, in each direction were 0.96, 0.93, and 0.82. Table S1 shows the final coordinates of the atoms used for the FEFF calculations. In our proposed model, a central Ni atom in the Ni trimer was bound to the oxygen atoms along the [001] step and was located above a bridging oxygen in the lower terrace (O_L). The central Ni–O distances were 0.206 nm for the [$1\bar{1}0$] direction (denoted as Ni2–O_U2 in Figure 6) and 0.211 nm for the [110] direction (denoted as Ni2–O_L2 in Figure 6). Two Ni atoms were bound to the central Ni atom along the [001] direction forming a Ni trimer. Ni–Ni distances were 0.260 nm and the bond angle was 167º. The Ni–O_U and Ni–O_L distances in both ends of the Ni trimer were 0.202 and 0.205 nm, respectively. In our previous paper, we found the Ni–O_U and Ni–O_L distances in the Ni monomer to be 0.199 and 0.204 nm, respectively [29, 31]. The distances were a little longer than those of the monomer but all Ni–O_U distances were shorter than the Ni–O_L in the trimer, reflecting the original TiO_2 structure.

Here, we evaluated the tolerance level of the proposed structure ($R < 1$) by changing the Ni atom positions, as shown in Figure 7, in three different ways. (1) When the Ni1 and Ni3 coordinates were changed in the [001] direction from the original structure, the Ni1(or Ni3)–Ni2 bond range of 0.258 to 0.261 nm was acceptable (Figure 7a). (2) When the Ni_3 coordinates were moved along the [$1\bar{1}0$] direction while maintaining the relative positions of the three Ni atoms, the Ni2–O_U2 bond range of 0.205 to 0.207 nm was acceptable (Figure 7b). (3) When the Ni_3 coordinates were moved along the [110] direction while maintaining the relative positions of the three Ni atoms, the Ni2–O_L2 bond range of 0.205 to 0.214 nm was acceptable (Figure 7c). The Ni–O distance along the [$1\bar{1}0$] and [110] directions could be determined with an error of ± 0.002 and ± 0.005 nm, respectively. All of the bond lengths around the Ni atoms are summarized in Figure 6d. The observed Ni–Ni bond length (0.260 ± 0.002 nm) was longer than that of the Ni^0 metal bond (typically 0.250 nm) but shorter than the Ti–Ti distance in the TiO_2 lattice.

The highly-stepped TiO_2(110) surface had coordinatively unsaturated in-plane and bridging oxygens with their dangling bonds directed to Ti vacancies. In our previous paper, we proposed that the vacant cation site was the stable adsorption site for the Ni metal atoms [29-31]. Accordingly, Ni is trapped by dangling bonds of these coordinative unsaturated oxygens. Owing to the stabilization imparted by bridging oxygen atoms from the bottom and in-plane oxygen atoms from the side, a longer Ni–Ni distance was observed. Such a longer Ni–Ni distance may prevent further growth in the [001] direction due to the lattice mismatch. The Ni trimer with a Ni–Ni distance of 0.260 nm was stabilized by the Ni–O interactions. Additionally, further growth of Ni clusters might be limited because the mismatching of O–O (0.296 nm) and Ni–Ni (0.260 nm) became too large. There are several Ni trimers reported in the literature, as described in Table S2. The linear Ni_3 compounds have

distances ranging from 0.236 to 0.283 nm depending on the structure and valence states; the linear structure can be achieved through ligand stabilization. The Ni trimer at the step site of TiO_2(110) was just in this range and was stabilized by the interaction with the step edge. The trimer was the nucleus for further cluster growth at the step, as was observed by STM in previous studies [33, 50, 51]. We are performing the DFT calculation to confirm the Ni trimer structure at the step.

One drawback of the adsorption structure of Ni proposed here is the origin of the oxygen atoms (O_u4 in Figure 6) along the [001] step which fixed the Ni trimer species on the surface. The adsorption site corresponds to the oxygen site bound to Ti with a single bond (position 1 in Figure 13 in Ref. [23]). However, as pointed out by Diebold [23], these oxygen atoms should be unstable. We need further experimental and theoretical studies also on this point.

In summary, we deposited Ni on a highly-stepped TiO_2(110) surface to understand the effect of the step site on the metal growth and the metal structure. PTRF-XAFS investigation indicated that small Ni cluster with a hemispherical shape (1 nm and 0.8nm in lateral and vertical directions, respectively when 0.8 ML were deposited. An anisotropic Ni trimer species was formed at the [001] step for a deposition thickness of 0.07 ML. The Ni–Ni distance was longer than that in the Ni metal and the Ni trimer species had a strong interaction with oxygen at the [001] step edge, which resulted in a longer Ni–Ni distance and stabilization of the Ni trimer. We revealed that the surface modification to enhance the metal-anion interaction can control the deposited structure.

Acknowledgment

The work was carried out under the approval of the Photon Factory advisory committee (PAC No. 2007G594, 2008G603, 2008G604). This work was financially supported by Grant-in-Aid for Scientific Research in Priority Areas “Nano functional element 474” and supported by a NEDO (New Energy and Industrial Technology Development Organization) project.

References

[1] P. Jiang, S. Porsgaard, F. Borondics, M. Kober, A. Caballero, H. Bluhm, F. Besenbacher, M. Salmeron, J Am Chem Soc, 132 (2010) 2858-+.

[2] M. Ichikawa, Adv Catal, 38 (1992) 283-400.

[3] H.J. Freund, Faraday Discuss, 114 (1999) 1-31.

[4] H.J. Freund, Surf Sci, 500 (2002) 271-299.

[5] H.G. Boyen, G. Kastle, F. Weigl, B. Koslowski, C. Dietrich, P. Ziemann, J.P. Spatz, S. Riethmuller, C. Hartmann, M. Moller, G. Schmid, M.G. Garnier, P. Oelhafen, Science, 297 (2002) 1533-1536.

[6] N. Toshima, Metal Nanoparticles Used as Catalysts, in: Dekker Encyclopedia of

Nanoscience and Nanotechnology - Six Volume Set (Print Version), CRC Press, 2004.
[7] A.C. Templeton, M.P. Wuelfing, R.W. Murray, Accounts Chem. Res., 33 (2000) 27-36.
[8] S.T. Zheng, D.Q. Yuan, H.P. Jia, J. Zhang, G.Y. Yang, Chem. Commun., (2007) 1858-1860.
[9] S.S. Feng, M.L. Zhu, L.P. Lu, L. Du, Y.B. Zhang, T.W. Wang, Dalton Trans., (2009) 6385-6395.
[10] H.J. Freund, M. Bäumer, H. Kuhlenbeck, Catalysis and surface science: What do we learn from studies of oxide-supported cluster model systems?, in: H.K. Bruce C. Gates (Ed.) Adv Catal, Academic Press, 2000, pp. 333-384.
[11] G. Ertl, H. Knözinger, J. Weitkamp, in: Handbook of Heterogeneous Catalysis, Wiley-VCH, Weinheim 1997.
[12] K.K. Bando, K. Asakura, H. Arakawa, K. Isobe, Y. Iwasawa, J. Phys. Chem., 100 (1996) 13636-13645.
[13] K. Asakura, K.K. Bando, Y. Iwasawa, J. Chem. Soc.-Faraday Trans., 86 (1990) 2645-2655.
[14] J.R.B. Gomes, J.P.P. Ramalho, F. Illas, Surf Sci, 604 (2010) 428-434.
[15] S.C. Ammal, A. Heyden, J Chem Phys, 133 (2010).
[16] A. Locatelli, T. Pabisiak, A. Pavlovska, T.O. Mentes, L. Aballe, A. Kiejna, E. Bauer, J Phys-Condens Mat, 19 (2007).
[17] A. Sasahara, K. Hiehata, H. Onishi, Catal Surv Asia, 13 (2009) 9-15.
[18] J.L. Zhang, M. Zhang, Y. Han, W. Li, X.K. Meng, B.N. Zong, J Phys Chem C, 112 (2008) 19506-19515.
[19] S. Suzuki, Y. Koike, K. Fujikawa, N. Matsudaira, M. Nakamura, W.J. Chun, M. Nomura, K. Asakura, Catal Today, 117 (2006) 80-83.
[20] S. Suzuki, Y. Koike, K. Fujikawa, W.J. Chun, M. Nomura, K. Asakura, Chem Lett, 33 (2004) 636-637.
[21] W.J. Chun, Y. Tanizawa, T. Shido, Y. Iwasawa, M. Nomura, K. Asakura, J Synchrotron Radiat, 8 (2001) 168-172.
[22] K. Asakura, Polarization-dependent total reflection fluorescence extended X-ray absorption fine structure and its application to supported catalysis, in: Catalysis, The Royal Society of Chemistry, 2012, pp. 281-322.
[23] U. Diebold, Surf Sci Rep, 48 (2003) 53-229.
[24] W.J. Chun, K. Asakura, Y. Iwasawa, Chem Phys Lett, 288 (1998) 868-872.
[25] W.J. Chun, K. Asakura, Y. Iwasawa, Journal of Physical Chemistry B, 102 (1998) 9006-9014.
[26] W.J. Chun, K. Asakura, Y. Iwasawa, Catal Today, 44 (1998) 309-314.
[27] K. Asakura, W.J. Chun, Y. Iwasawa, Jpn J Appl Phys 1, 38 (1999) 40-43.

[28] Y. Tanizawa, T. Shido, W.J. Chun, K. Asakura, M. Nomura, Y. Iwasawa, Journal of Physical Chemistry B, 107 (2003) 12917-12929.
[29] Y. Koike, W.J. Chun, K. Ijima, S. Suzuki, K. Asakura, Mater Trans, 50 (2009) 509-515.
[30] K. Ijima, Y. Koike, W.J. Chun, Y. Saito, Y. Tanizawa, T. Shido, Y. Iwasawa, M. Nomura, K. Asakura, Chem Phys Lett, 384 (2004) 134-138.
[31] Y. Koike, K. Ijima, W.J. Chun, H. Ashima, T. Yamamoto, K. Fujikawa, S. Suzuki, Y. Iwasawa, M. Nomura, K. Asakura, Chem Phys Lett, 421 (2006) 27-30.
[32] Y. Koike, K. Fujikawa, S. Suzuki, W.J. Chun, K. Ijima, M. Nomura, Y. Iwasawa, K. Asakura, J Phys Chem C, 112 (2008) 4667-4675.
[33] J. Zhou, Y.C. Kang, D.A. Chen, Surf Sci, 537 (2003) L429-L434.
[34] E. Wahlstrom, N. Lopez, R. Schaub, P. Thostrup, A. Ronnau, C. Africh, E. Laegsgaard, J.K. Norskov, F. Besenbacher, Phys Rev Lett, 90 (2003).
[35] C. Xu, X. Lai, G.W. Zajac, D.W. Goodman, Phys Rev B, 56 (1997) 13464-13482.
[36] A. Sasahara, C.L. Pang, H. Onishi, Journal of Physical Chemistry B, 110 (2006) 13453-13457.
[37] J.F. Sanz, A. Marquez, J Phys Chem C, 111 (2007) 3949-3955.
[38] K. Okazaki-Maeda, Y. Maeda, Y. Morikawa, S. Tanaka, M. Kohyama, Mater Trans, 47 (2006) 2663-2668.
[39] B.K. Min, W.T. Wallace, D.W. Goodman, Surf Sci, 600 (2006) L7-L11.
[40] S.C. Parker, A.W. Grant, V.A. Bondzie, C.T. Campbell, Surf Sci, 441 (1999) 10-20.
[41] Q.H. Zeng, K. Wong, X.C. Jiang, A.B. Yu, Appl. Phys. Lett., 92 (2008).
[42] M.S. Chen, D.W. Goodman, Top. Catal., 44 (2007) 41-47.
[43] A. Sasahara, C.L. Pang, H. Onishi, The Journal of Physical Chemistry B, 110 (2006) 17584-17588.
[44] K. Okazaki, Y. Morikawa, S. Tanaka, K. Tanaka, M. Kohyama, Phys Rev B, 69 (2004) 235404.
[45] W.J. Chun, K. Miyazaki, N. Watanabe, Y. Koike, S. Takakusagi, K. Fujikawa, M. Nomura, K. Asakura, J Ceram Soc Jpn, 119 (2011) 890-893.
[46] A.L. Ankudinov, B. Ravel, J.J. Rehr, S.D. Conradson, Phys Rev B, 58 (1998) 7565-7576.
[47] H. Oyanagi, Z.H. Sun, Y. Jiang, M. Uehara, H. Nakamura, K. Yamashita, Y. Orimoto, L. Zhang, C. Lee, A. Fukano, H. Maeda, J Appl Phys, 111 (2012).
[48] B. Domenichini, F. Sutara, T. Skala, V. Matolin, S. Bourgeois, J Electron Spectrosc, 184 (2011) 410-413.
[49] H. Onishi, T. Aruga, C. Egawa, Y. Iwasawa, Surf Sci, 233 (1990) 261-268.
[50] J. Zhou, D.A. Chen, Surf Sci, 527 (2003) 183-197.
[51] R.E. Tanner, I. Goldfarb, M.R. Castell, G.A.D. Briggs, Surf Sci, 486 (2001) 167-184.

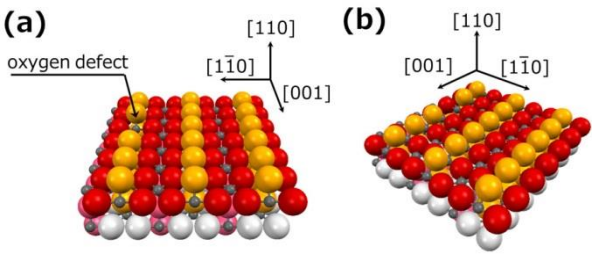

Figure 1. Schematic illustration of TiO_2(110) surface showing oxygen defects. Large and small balls correspond to oxygen and titanium atoms, respectively. Red: in-plane oxygen on the upper terrace (O_U); light grey: in-plane oxygen on the lower terrace; Orange: bridging oxygen on the upper terrace; and pink: bridging oxygen on the lower terrace (O_L).

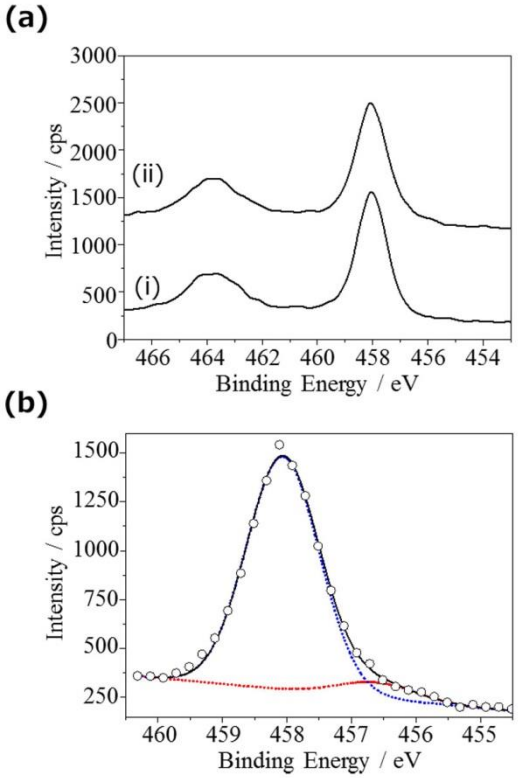

Figure 2. (a) XP spectra of the Ti 2p region for TiO_2(110) after annealing at (i) 900 K and (ii) 823 K. An offset of 1000 cps was applied to the data of (ii) for clarity. (b) An enlarged XP spectrum of Ti $2p_{3/2}$ region with peak deconvolution for the 823 K annealed sample. The main peak at 458 eV (blue dotted line) corresponds to Ti^{4+} and the shoulder peak at 456.5 eV (red dotted line) corresponds to Ti^{3+}. Open circles and the black solid line show experimental data and the summation of Ti^{4+} and Ti^{3+}, respectively.

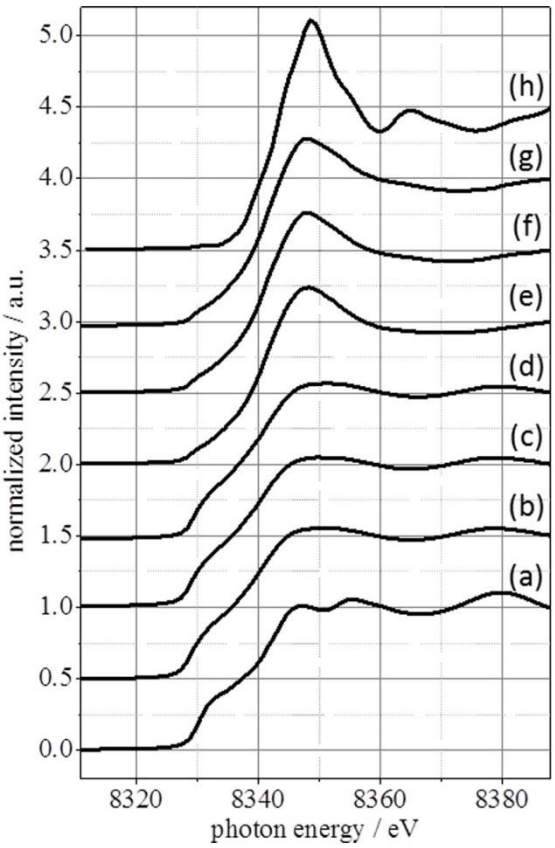

Figure 3. Normalized Ni K edge polarization dependent XANES spectra of Ni species on the highly-stepped TiO_2(110) surface. (a) Ni foil, (b-d) 0.8 ML Ni species, (e-g) 0.07 ML Ni (h) NiO. (b,e) *E*//[001], (c,f) *E*//[1$\bar{1}$0], (d,g) *E*//[110].

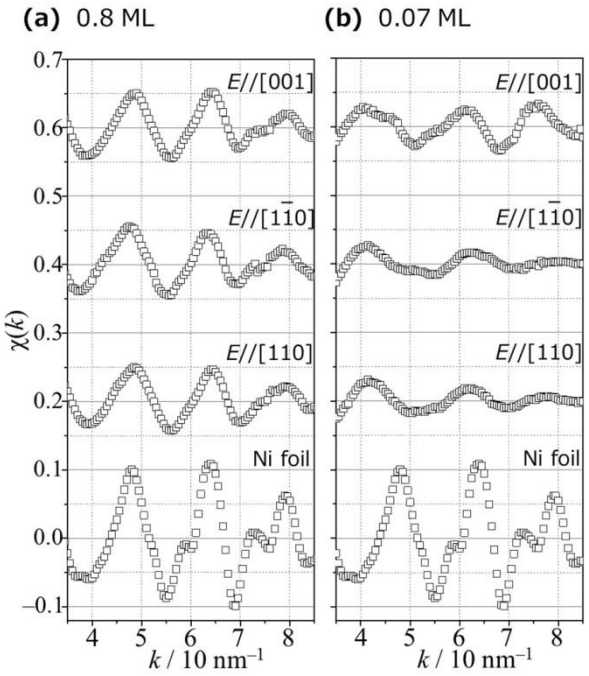

Figure 4. Normalized Ni K edge PTRF-XAFS oscillations for (a) 0.8 ML samples and (b) 0.07 ML samples. Normalized Ni K edge XAFS oscillations for Ni foil are also indicated at the bottom.

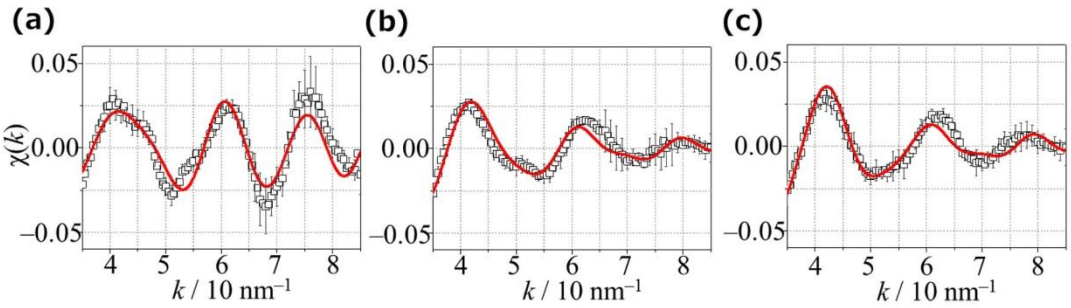

Figure 5. Normalized Ni K edge PTRF-XAFS oscillations for the 0.07 ML sample showing error bars; (a) *E*//[001] (b) *E*//[1$\bar{1}$0] (c) *E*//[110]. Red lines are the oscillations simulated using the FEFF code.

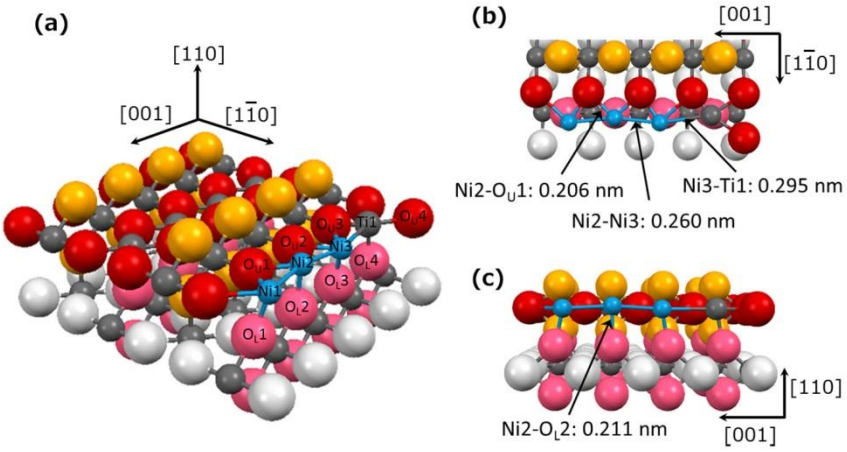

(d)

bond	*r* / nm
Ni1-O_U1	0.202
Ni3-O_U3	
Ni2-O_U1	0.206
Ni2-O_U2	
Ni3-O_U3	0.251
Ni1-O_L1	0.205
Ni3-O_L3	
Ni2-O_L2	0.211

Figure 6. (a-c) Schematic illustration of proposed anisotropic Ni trimer on a highly-stepped TiO_2(110) surface. Large balls correspond to oxygen atoms. Small gray and blue balls correspond to Ti atoms and Ni, respectively. Red: in-plane oxygen on the upper terrace (O_U); light grey: in-plane oxygen on the lower terrace; orange: bridging oxygen on upper terrace; and pink: bridging oxygen on the lower terrace (O_L). (d) Summary of Ni‑O bonds.

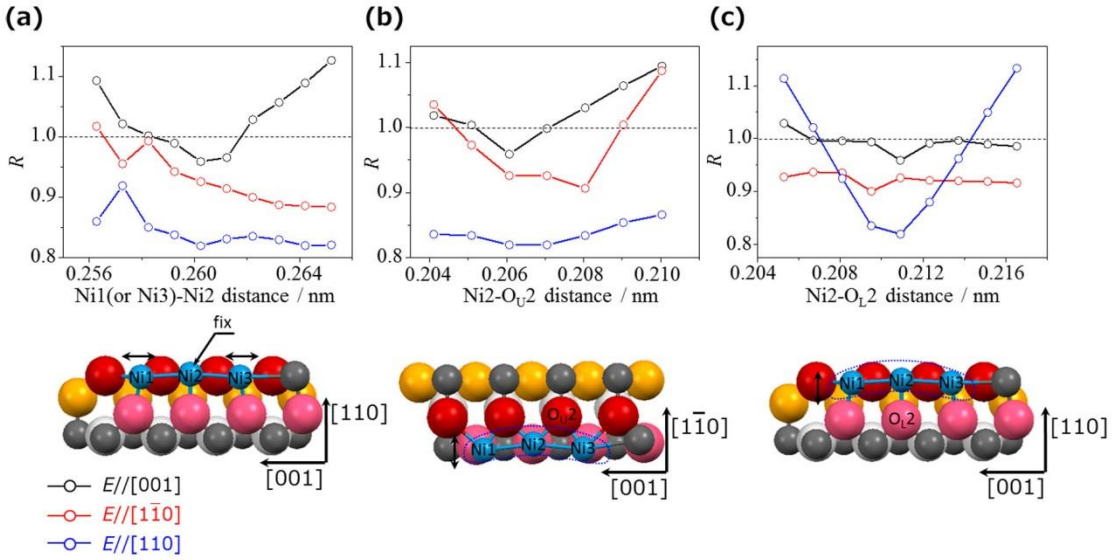

Figure 7. *R* value as a function of the Ni coordinate. *R* value calculated for the *E*//[001] direction, *E*//[1$\bar{1}$0] direction and *E*//[110] direction are shown in black, red, and blue, respectively. (a) Ni1 and Ni3 coordinates were symmetrically changed along the [001] direction. (b) Ni trimer cluster was moved along the [1$\bar{1}$0] direction while holding the three Ni relative positions constant (c). Ni trimer cluster was moved along the [110] direction while holding the three Ni relative positions constant.

Table 1

Polarization	bond	r / nm	N_{eff}
E // [001]	Ni-Ni	0.246 ±0.004	5.4 ±0.4
E // [1$\bar{1}$0]	Ni-Ni	0.246 ±0.004	5.3 ±0.4
E // [110]	Ni-Ni	0.246 ±0.004	4.4 ±0.3

[a] The FT range in the k space was from 0.30 to 1.30 nm^{-1}

[b] Phase shift and back scattering amplitude estimated from Ni foil was used for curve fitting

[c] σ and ΔE_0 were fixed at 0.06 and –5.0, respectively.

Anisotropic Growth of Ni Trimer Formed on a Highly-stepped TiO_2(110) Surface

Hiromitsu Uehara,[a] Muhammad Haneef bin Hanaffi,[a] Yuichiro Koike,[a] Keisuke Fujikawa,[a] Shushi Suzuki,[a,b] Hiroko Ariga,[a] Satoru Takakusagi,[a] Wang-Jae Chun, [c] Yasuhiro Iwasawa,[d] and Kiyotaka Asakura[*,a]

Supplementary Information

Supplementary Information contains a LEED pattern, an STM image and XP spectrum of highly-stepped TiO_2(110) surface (Figure S1, Figure S2 and Figure S3, respectively), coordinates of the Ni_3 and TiO_2(110) substrate which connect directly to the Ni trimer cluster (Table S1) and the summary of Ni–Ni distances found in different Ni trimer compounds(Table S2).

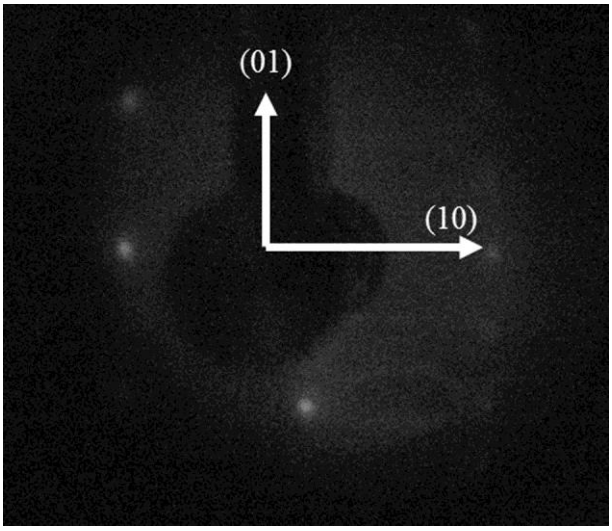

Figure S1. LEED pattern of 823 K annealed TiO_2(110) after Ar ion sputtering. Electron energy = 80 eV

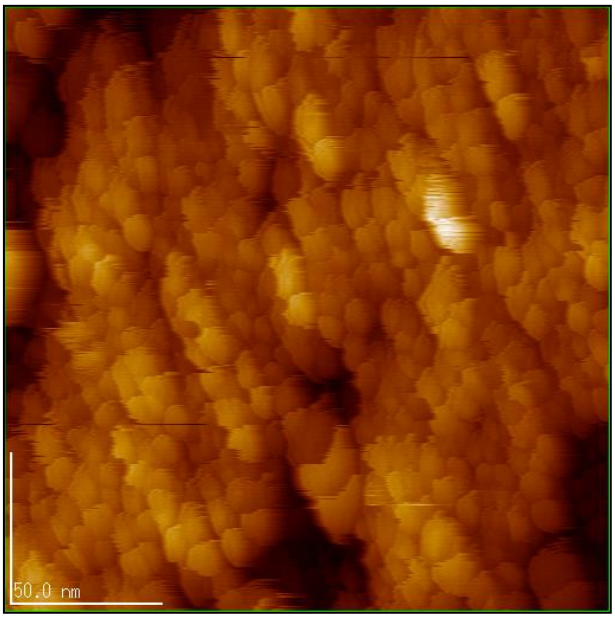

Figure S2. STM picture of 823 K annealed TiO_2(110) after Ar ion sputtering. Sample bias = 2 V, Sample current =100 pA.

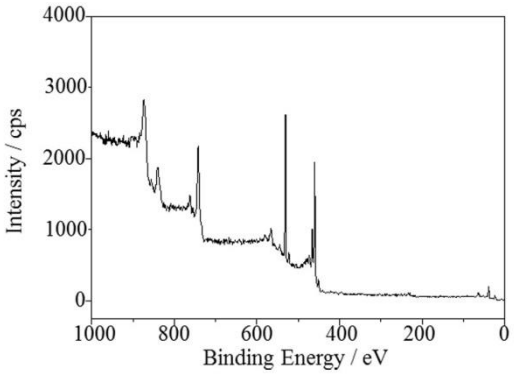

Figure S3. XP spectrum of 823 K annealed TiO_2(110) after Ar^+ ion sputtering.

Table S1 Coordinate of Ni trimer and TiO_2(110) support surface directly connected to the Ni trimer.

Atoms	X	Y	Z
Ni	0.12811	−0.49189	−3.62982
Ni	−0.15989	−0.40688	−1.04482
Ni	0.12812	−0.49188	1.54019
O	−1.09259	0.68282	3.39368
O	1.17562	1.22552	−4.00382
O	−1.09259	0.68282	−2.52432
O	1.17561	1.22551	−1.04482
O	−1.09259	0.68282	0.43469
O	1.17561	1.22552	1.91418
Ti	−0.20138	−0.20838	4.45518

Table S2 Ni–Ni distances found in different Ni trimer compounds.

Compound	structure	Ni–Ni/nm	Reference
$[(Ni\text{-}Ni\text{-}Ni)@(Ge_9)_2]^{4-}$	Linear	0.24	[S1]
Bis(acetylacetonato)Ni(II)	Linear	0.289	[S2]
$[Ni_3(edt)_4]^{2-}$	Linear	0.283	[S3]
$[Ni_9(CO)_{18}]^{2-}$	Triangle	0.237-0.240	[S4]
$(Ph_4P)_2[Ni_3(SCH(CH_3)COO)_4]$	Linear	0.278	[S5]
Free Ni_3 (Calculation)	Triangle	0.221	[S6]

[S1]J.M. Goicoechea, S.C. Sevov, Angewandte Chemie, 117 (2005) 4094-4096.

[S2] G.J. Bullen, R. Mason, P. Pauling, Inorganic Chemistry, 4 (1965) 456-462.

[S3] J.R. Nicholson, G. Christou, J.C. Huffman, K. Folting, Polyhedron, 6 (1987) 863-870.

[S4] D.A. Nagaki, L.D. Lower, G. Longoni, P. Chini, L.F. Dahl, Organometallics, 5 (1986) 1764-1771.

[S5] S.G. Rosenfield, M.L.Y. Wong, D.W. Stephan, P.K. Mascharak, Inorganic Chemistry, 26 (1987) 4119-4122.

[S6] H. Johll, J. Wu, S.W. Ong, H.C. Kang, E.S. Tok, Phys Rev B, 83 (2011)205408